catalysts

MDPI

Article

Plasmonic-Assisted Water–Gas Shift Reaction of Gold Particles on TiO_2

Ahmed Khaja Wahab [1], Kumudu Mudiyanselage [2,†] and Hicham Idriss [3,*]

[1] Department of Chemical Engineering, University of Waterloo, Waterloo, ON N2L 3G1, Canada; kwahmed@uwaterloo.ca
[2] Surface Science and Advanced Characterization, SABIC-CRD at King Abdullah University for Science and Technology (KAUST), Thuwal 23955, Saudi Arabia; kumudu.mudiyanselage@albemarle.com
[3] Institute of Functional Interfaces, Karlsruhe Institute of Technology (KIT), 76344 Eggenstein-Leopoldshafen, Germany
* Correspondence: hicham.idriss@kit.edu
† Current address: Albemarle Corporation, Corporate Headquarters, 4250 Congress Street, Suite 900, Charlotte, NC 28209, USA.

Abstract: The Localized Surface Plasmon (LSP) effect of 5 nm mean size Au particles deposited on TiO_2 P25 was investigated during the photo-thermal water gas shift reaction (WGSR). The effects of CO concentration, excitation light flux and energy, and molecular oxygen addition during the reaction were investigated. The photocatalytic WGSR rate under light excitation with wavelengths extending from 320 to 1100 nm was found to be higher than the thermal reaction alone at the same temperature (85 °C). A H_2/CO_2 ratio of near unity was found at high concentrations of CO. The addition of molecular oxygen during the reaction resulted in a slight decrease in molecular hydrogen production, while the rates of CO_2 formation and CO consumption changed by one order of magnitude. More importantly, it was found that the WGSR rates were still high under only visible light excitation (600–700 nm). The results prove that Au LSP alone triggers this chemical reaction without requiring the excitation of the semiconductor on which they are deposited.

Keywords: Au/TiO_2 P25; localized surface plasmon (LSP); photo-thermal water–gas shift reaction (WGSR); hydrogen production; preferential oxidation reaction (PROX)

Citation: Wahab, A.K.; Mudiyanselage, K.; Idriss, H. Plasmonic-Assisted Water–Gas Shift Reaction of Gold Particles on TiO_2. *Catalysts* **2023**, *13*, 1444. https://doi.org/10.3390/catal13111444

Academic Editors: Hatem Amin, Yasser Hassan and Hassan A. Alhazmi

Received: 18 October 2023
Revised: 10 November 2023
Accepted: 13 November 2023
Published: 15 November 2023

1. Introduction

The water–gas shift reaction (WGSR) is one of the important industrial processes for adjusting the CO to H_2 ratio for methanol synthesis and for producing high-purity H_2 for ammonia synthesis. In the WGSR, CO(g) reacts with H_2O(g), forming CO_2(g) and H_2(g).

$$CO(g) + H_2O(g) \rightarrow CO_2(g) + H_2(g) \quad \Delta H = -41.1 \text{ kJ/mol}$$

The WGSR is performed at low (190–250 °C) and high (400–500 °C) temperatures with Cu/ZnO and Fe_2O_3-based catalysts, respectively [1]. At high temperatures, the CO conversion is equilibrium-limited, and, at low temperatures, the reaction is kinetically limited.

In addition to iron- and copper-based catalysts, precious-metal (Au, Pt, and Pd)-containing catalysts have been investigated for WGSR at low temperatures [1–4]. Previous studies found a much higher WGSR activity of gold nanoparticles on reducible supports such as TiO_2 and CeO_2 than that on Al_2O_3 and SiO_2 [3,5]. Among these catalysts, Au/TiO_2 showed comparable WGSR activity to that of commercial $Cu/ZnO/Al_2O_3$ catalysts [2]. It has also been proposed that the WGSR on Au-based catalysts takes place at the interfacial sites [5,6]. The proposed active interfacial site on Au/TiO_2 is $Au^{\delta-}\_O_V\_Ti^{3+}$ (O_V: oxygen vacancy), where electron-enriched $Au^{\delta-}$ species enhance CO chemisorption, while $O_V\_Ti^{3+}$ contributes to the dissociation of water [5].

Mainly, two reaction mechanisms, redox (also called regenerative) and associative, have been proposed for the WGSR [7]. In the redox mechanism, CO reacts with the lattice O of the catalyst, forming CO_2 and creating vacant sites. Then, H_2O dissociates, filling the vacant sites, whereas the two protons of water take the two electrons left upon the creation of the vacancy and thus make one hydrogen molecule. In the associative mechanism, intermediate species are formed from the reaction between CO and surface -OH species derived from the dissociation of water. The proposed intermediates in previous studies are formate species (HCOO(a)) [3,8], carbonate-like species, and carboxyl (HOCO) [9], which decompose, forming CO_2 and H_2. In some studies, formates and carbonate-like species have been reported to be spectators [10,11]. To our knowledge, the carboxyl species has not been observed experimentally on Au/TiO_2.

The redox mechanism usually takes place at high temperatures, whereas the associative mechanism occurs at low temperatures. However, density functional theory (DFT) calculation results have indicated that it is difficult for carboxyl species to form during the WGSR on Au/TiO_2 catalysts at low temperatures. It was also found that formates are too stable to release H_2, and hence it was suggested that the redox mechanism is the primary reaction pathway at low temperatures [12]. Another DFT computation study on the WGSR mechanism over Au_{10}, Au_{13}, and Au_{20} clusters reported that the carboxyl mechanism occurred over Au_{10} and Au_{20} clusters, while the redox mechanism took place over the most active Au_{13} cluster [13]. Despite these theoretical studies, the associative mechanism is still widely accepted as the pathway of the WGSR at low temperatures.

On precious-metal/TiO_2 catalysts such as Au/TiO_2 [14], Pt/TiO_2 [4,15], and Pd/TiO_2 [16], not only thermal but also photo-assisted WGSRs have been studied. A photo-catalytic WGSR at low or ambient temperatures offers economical and environmental advantages. In particular, H_2/CO_2 would be generated at a desired ratio via a cleaner process using sunlight as an energy source. It has been proposed that the photo-asssited WGSR on M(Au, Pd, and Pt)/TiO_2 occurs at the M/TiO_2 interface [16], similar to the thermal WGSR [8]. However, the photocatalytic WGSR over Pt/TiO_2 and Pd/TiO_2 occurs efficiently only at very low concentrations of CO. At high concentrations of CO, the rates of H_2 and CO_2 production decrease. There is a net negative effect on activity upon increasing the concentration of CO due to the strong adsorption of CO on Pt or Pd [15,16]. Au/TiO_2 may function without a negative effect on the activity at higher CO concentrations due to the weak CO adsorption on Au particles.

Au/TiO_2 catalysts have also been reported to show catalytic activity for CO oxidation at low temperatures [17]. Thermal CO oxidation on Au/TiO_2 has been proposed to occur predominantly through a Au-assisted Mars–van Krevelen (MvK) mechanism for reaction temperatures of 80 °C and above [18]. In the MvK mechanism, first, CO molecules adsorb on Au particles and then abstract TiO_2 lattice oxygen at the Au/TiO_2 interface; finally, CO_2 molecules desorb, forming oxygen vacancies and reduced Au/TiO_{2-x}. The next step in the Au-assisted MvK mechanism is the re-oxidation of the previously reduced catalyst [18]. Green et al. also proposed that CO oxidation on Au/TiO_2 occurred on metal sites at the Au/TiO_2 interface [19]. It has also been shown that O-O bond scission is activated by the formation of a CO-O_2 complex at the Au/TiO_2 interface [17,19]. Moreover, the performance of Au/TiO_2 catalysts for CO oxidation improves in the presence of water [20]. A water-mediated reaction mechanism for room-temperature CO oxidation over Au/TiO_2 catalysts has been proposed [21]. DFT calculations showed that proton transfer at the Au/TiO_2 interface facilitates O_2 activation and binding, leading to the formation of Au–OOH that readily reacts with adsorbed CO on Au, forming Au–COOH. Au–COOH decomposes and forms hydrogen and CO_2.

Previous studies have also shown the preferential oxidation (PROX) of CO in the presence of H_2 on Au/TiO_2 [20,22–25]. The PROX reaction of CO on Au/TiO_2 in the presence of light irradiation has also been reported previously [26–28]. The UV irradiation of Au/TiO_2 promotes the preferential oxidation of CO in a H_2-rich stream [27]. The chemisorption of CO on Au/TiO_2 was enhanced by UV irradiation, but the chemisorption of H_2 was sup-

pressed on both TiO_2 and Au surfaces. It has been reported that PROX reaction rates were increased by up to a factor of 3 when Au/TiO_2 was irradiated by visible or UV light [26]. Yoshida et al. reported that the PROX rates of CO on Au/TiO_2 under dark conditions increased in the presence of UV–visible light due to the effect of charge separation due to localized surface plasmon resonance (LSPR) and the promoted electron transfer to the adsorbed O_2 [26]. It has also been proposed that the photo-generated electrons from TiO_2 cause changes in the chemisorbed energy of CO, H_2, and O_2 on Au/TiO_2 in a manner that promotes the preferential oxidation of CO in a H_2-rich stream [27].

Localized surface plasmons resonance (LSPR) are oscillations of free electrons. These are confined to the surface of gold nanoparticles (among other materials). Upon resonance, the charge oscillations create an intense local electric field (EF) on the surfaces of these nanoparticles. These oscillations have been studied in order to enhance the photocatalytic activity of semiconductors such as TiO_2 [29–32]. The effect on enhancing the reaction rate was found to be generally weak. The mechanism by which plasmonic metal nanoparticles improve energy conversion can be seen as a photonic or electronic effect. Photonic enhancement occurs through far-field scattering or near-field enhancement, while an electronic effect occurs via increasing local generation of electron hole pairs through direct electron transfer or resonant energy transfer, directly exciting electron–hole pairs non-radiatively through the relaxation of the surface plasmon dipole.

Overall there are many studies on thermal WGSRs [5,10,33–36] and the PROX of CO [20,22,24,37,38] on Au/TiO_2, but only a few investigations have reported on photo-assisted WGSRs [14] and the PROX of CO [26,27], and further studies are required to acquire a fundamental understanding of these reactions. We have opted to study an unusually high loading of Au (8 wt.%) on TiO_2 P25. We have previously studied a series of different Au wt.% on this support [39]; in these studies, Au particles were deposited via the deposition precipitation method [40]. This is particularly important in order to enhance their LSPR effect when compared to the semiconductor-alone (band gap) effect. In this study, we investigated the photo-assisted WGSR and the PROX of CO on 8 wt.% Au/TiO_2 at 85 °C.

2. Results and Discussion

We have previously studied a family of Au/TiO_2 P25 catalysts in some detail [39,41,42]. These studies included core and valence-level spectroscopy, XRD, photo-luminescence, UV-Vis absorbance, TEM, and EXAFS. Here, we give a brief description of the relevant information related to the present study. Figure 1 presents selected data replotted from ref. [39]. Figure 1A presents the UV-Vis of TiO_2 P25 without and with different gold loadings from 0.5 to 10 wt.%. TiO_2 P25 contains about 80–20 of anatase and rutile, with their band gaps being 3.2 (385 nm) and 3.0 (410 nm), respectively; here, only the edge is shown for simplicity. The absorbance due to gold plasmons (localized surface plasmon (LSP) of Au nanoparticles) starts at about 100 nm after the band gap of TiO_2. The LSP is centered at about 560 nm. Its intensity increases non-linearity with increasing Au coverage and becomes wider. A widening of the peak is seen at both energy sides (towards the IR and UV regions). It should be noted that the particles, even at 8–10 wt.%, are not touching each other; they are still dispersed on the surface. The TEM images in the insets show largely round particles from which an average size of 5.1 nm was extracted. Figure 1B shows XPS Au4f data of the same series. The binding energies at about 83.6 and 87.3 eV are for $Au4f_{7/2}$ and $Au4f_{5/2}$, respectively. Their peak areas increase linearly with increasing coverage and all have a small shift of about 0.2–0.4 eV to lower energy levels (when compared to bulk Au at 84.0 eV). The slight shift to lower energy might have been due to interfacial charge transfer or band bending and has not been corrected. The 8 wt.% corresponded to about 3 at.%. Recall that XPS presents the surface and near-surface atoms only and therefore the extracted number differs from that found for bulk. Figure 1C presents the valence band of the same series. It contains, in addition to the O2p structure in the 3–9 eV range (for pure TiO_2), the Au5d band when Au is present. The Fermi level was determined to be at the Au6s band binding energy position. This is more pronounced for the highly loaded

catalysts. The catalyst used in this study is therefore composed of Au particles (5.1 nm average size), largely in a metallic state (XPS Au4f, Au6d binding energy position), with 3 at. % and with a pronounced plasmon centered at about 560 nm and extending from 400 to 900 nm. The XRD patterns for the Au/P25 TiO_2 photocatalysts [35,39] are dominated by peaks due to anatase and rutile phases (85/15 weight ratio). Broad and weak signals were seen at 2θ = 44.4°, 65.6°, and 77.6°, which were due to Au (200), Au (220), and Au (311) reflections, respectively. The Au particles were of a mean size of 5.1 nm, these are extracted from counting a large number of particles in different like those presented in Figure S1A. Figure S1B,C show the expected (111) planes (*d* spacing = ca. 0.23 nm) of Au particles.

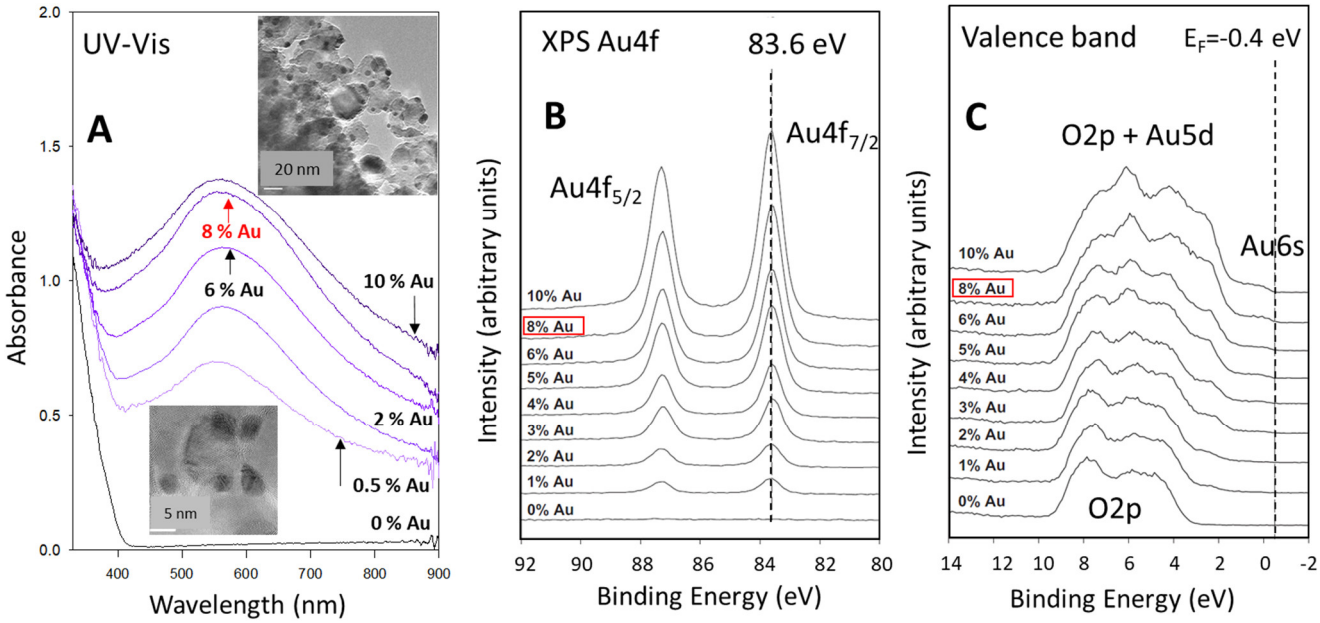

Figure 1. (**A**) UV-Vis-IR absorbance spectra of TiO_2 P25 and Au/TiO_2 P25 at the indicated atomic %. (**B**) XPS Au4f binding energy region of the series of Au-containing catalysts. All spectra show Au in a metallic state. (**C**) Valence band region of the same series shown in (**A**,**B**); in addition to the O2p region, a signal related to 5d and 6s orbitals/bands appear at high at. % of Au. The 8% Au/TiO_2 catalyst used in this study is indicated by the red color and red rectangles. The % refer to catalyst weigh. Figures were modified from ref. [39] with permission.

In the following, we present the thermal and photo-thermal photocatalytic reactions of CO and H_2O to CO_2 and H_2 over the 8 wt.% Au/TiO_2 P25 catalyst. In order to do so, we changed the excitation energy in order to probe the effect of Au LSPR on the reaction rate. In Figures S2–S8 in the Supporting Information, the fluxes and energies of the different light excitations used are given.

2.1. Photocatalytic Water–Gas Shift Reaction at ≈25 °C (Room Temperature)

First, we have investigated the photocatalytic WGSR at ≈25 °C. At this temperature, there was no contribution from thermal activity. The photons' energy extended from 320 nm to 1100 nm, and the light fluxes in the UV (320–400 nm), visible (400–800 nm), and IR (800–1100 nm) regions were 8, 67, and 62 mW/cm^2. The rates of production of H_2 and CO_2 were found to be equal to 3.6 × 10^{-8} and 4.6 × 10^{-8} moles/min, respectively. Similar results will be discussed in more detail in Section 2.3.

2.2. Thermal Water–Gas Shift Reaction

To identify the effect of temperature, the thermal WGSR at 85, 150, 200, and 250 °C was performed in the absence of light irradiation. In all the experiments, water was used in excess (with a ratio of [H_2O]/[CO] > 3), and [CO] was kept at 6.7 × 10^{-6} mol/mL. The H_2 production rate was found to be about 4.9 × 10^{-7} mol/min at 85 °C, whereas

it was 40 times higher, ca. 2×10^{-5} mol/min, at 250 °C. In these experiments, high concentrations of reactants were used so that the production rate would be less affected by changes in their concentration. Figure 2A,B show the production of H_2 and CO_2; CO consumption; and the Arrhenius plot for H_2 production from which an activation energy of 32.5 kJ/mol was extracted. The activation energy for industrial low-temperature and high-temperature water–gas shift reactions were reported to be 52 and 110 kJ/mol over CuZnO and Fe_3O_4-Cr_2O_3, respectively [43].

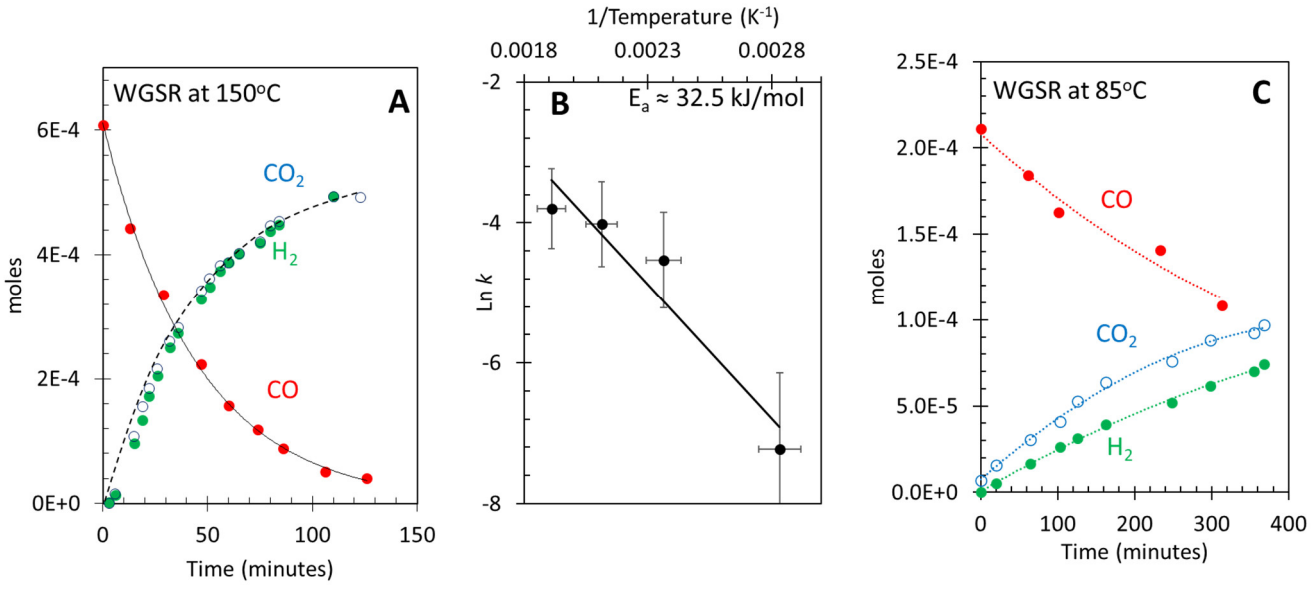

Figure 2. (**A**) CO consumption and H_2 and CO_2 production as a function of time at 150 °C during the WGSR reaction over 8 wt.% Au/TiO_2 P25. (**B**) Arrhenius plot for the hydrogen production rates of WGSR on the same catalyst. The rate constants are shown in Table 1. (**C**) H_2 and CO_2 formation and CO consumption during thermal WGSR at 85 °C.

In order to more accurately monitor the consumption of CO, the thermal WGSR was carried out with a lower initial concentration of CO, 5 mL of CO (2.2×10^{-4} moles/reactor volume or about 2×10^{-6} mol/mL)), and 20 µL of water at a temperature of 85 °C. The initial ratio of H_2O to CO in the gas phase was 3, and the results are presented in Figure 2C. The data show that the amounts of H_2 and CO_2 formed increased, whereas the amounts of CO decreased, with time. The rate of consumption of CO was 4.8×10^{-7} mol/min, and the initial rates of production of H_2 and CO_2 were 2.4×10^{-7} and 3.4×10^{-7} mol/min, respectively. The rate of CO consumption was found to be 1.4 times higher than the rate of production of CO_2, indicating that a fraction of CO converted to form adsorbed species, which do not further react to form CO_2. In addition, a small fraction of CO converted to CH_4 as evidenced by the detection of a trace amount of this compound via gas chromatography. However, the methanation of CO generally requires reaction temperatures greater than 573 K [26]. The initial ratio of H_2 to CO_2 production was about 0.85, which was calculated after subtracting the CO_2 formed by CO oxidation with the residual O_2 (~6×10^{-6} moles) present after purging the reactor. The observed H_2 to CO_2 ratio was lower than the expected value of 1.0, showing that H_2 is consumed by some side reactions, such as methanation to form CH_4, as discussed earlier, and reaction with residual O_2 to form H_2O. A ratio of H_2/CO_2 of less than 1.0 was reported by others for the WGSR on Au/TiO_2 [14] and Pt/TiO_2 [4]. The previously reported ratio of H_2 to CO_2 for a WGSR carried out on 1 wt.% Au/TiO_2 was 0.78, whereas it was in the range of 0.7–1.0 on Pt/TiO_2 with and without irradiation [4].

The thermal WGSR at 85 °C may take place via an associative mechanism described in the Introduction section. In the associative mechanism, first, intermediate species, such as formates, are formed at the Au/TiO_2 interface via the reaction between adsorbed

CO and surface OH groups, derived from the dissociation of H_2O, on TiO_2, as reported previously [8]. Thus, the formed intermediate species react to form H_2 and CO_2. Adsorbed formate species on catalyst surfaces have been detected in many studies via infrared spectroscopy and have been proposed to be intermediates [3,8].

The formation and decomposition of formates on Au/TiO_2 can be seen in the following.

$$CO\ (g) + H_2O\ (g) + O(s) \rightarrow CO(a) + OH(a) + OH(s) \quad (1)$$

The above reaction depicts the molecular and dissociative adsorption of CO and water, respectively.

$$CO(a) + OH(a) \rightarrow HCOO(a) \quad (2)$$

Formate formation

$$HCOO(a) \rightarrow CO_2 + [H(a)] \quad (3)$$

Formate decomposition

[ ] indicates that the species is a not stable intermediate

$$[H(a)] + OH(s) \rightarrow H_2(g) + O(s) \quad (4)$$

Hydrogen production

Here, (g), (s), and (a) stand for gas, surface, and adsorbed, respectively.

Deviation from stoichiometry between CO_2 and H_2 occurred at 85 °C for both CO concentrations investigated. This was not found at higher temperatures (at 150, 200, and 250 °C the ratio was ≈1). This might be linked to the formation of hydrogen in the reaction (Equation (4)). The following sentences may explain the reason for this. Strictly, one hydrogen molecule originates from the reaction of a hydride (upon the dissociation of the C–H of a formate) and a proton (upon the dissociation of a molecule of water). In other words, this is a recombination reaction with two distinctly different species (one hydrogen with two electrons (a hydride) and a proton). It is notable that a hydride was not seen on Ti cations of TiO_2 (this is the reason the brackets on Equation (3) are put, so it is considered a transition-state intermediate). On the other hand, CO_2 formation results from the direct decomposition of a formate species (Equation (3)). It is possible that during the recombination (of $H^-(a)$ and $H^+(a)$), the hydride loses one or two electrons to the lattice. When the temperature is increased, the species may have enough motion (thermal energy) to increase the reaction rate and prevent electron loss. These phenomena may explain the deviation of stoichiometry around a temperature of 85 °C.

Table 1. Hydrogen production rates at different temperatures during the WGSR over 8 wt.% Au/TiO_2 P25.

T (°C)	T (K)	1/T(K)	Rate (H_2 moles/min)
80	353	0.002832	4.87×10^{-7}
150	423	0.002363	8.69×10^{-6}
200	473	0.002113	9.00×10^{-6}
250	523	0.001911	1.97×10^{-5}

2.3. Photo-Assisted Water–Gas Shift Reaction at 85 °C: Effect of CO Concentration

Experiments were performed in the presence of light extending from the UV to IR regions (320–400; 400–750; 750–1100 nm). First, the effect of light intensity was studied while light energy was kept constant. This is shown in Figure 3A,B. The difference in the light flux between A and B was about two (for all light regions). The WGSR shows higher activity compared to the thermal reaction, at the same temperature, in both cases (two to three times higher). However, doubling the light intensity increased this activity by about 30%. We made no attempt to study the light intensity effect because our set up may

not be ideal for such an endeavor. The practical point to extract from this result is that slight variations in light flux reaching the catalyst from one experiment to the other (say, by 10%) would not dramatically affect the comparative study presented next. Again, as in the thermal reaction, the ratio of H_2 to CO_2 was less than the stoichiometric one and saturated faster than that of CO_2. Yet, increasing light intensity improved the ratio. At higher light intensity, the CO_2/H_2 ratio was closer to unity than that at low light intensity (about 0.9). Also, similar to the thermal WGSR, the rate of consumption of CO was 1.3 times higher than the rate of production of CO_2, indicating that a fraction of CO converted to form adsorbed species, which do not all further dissociate to form CO_2.

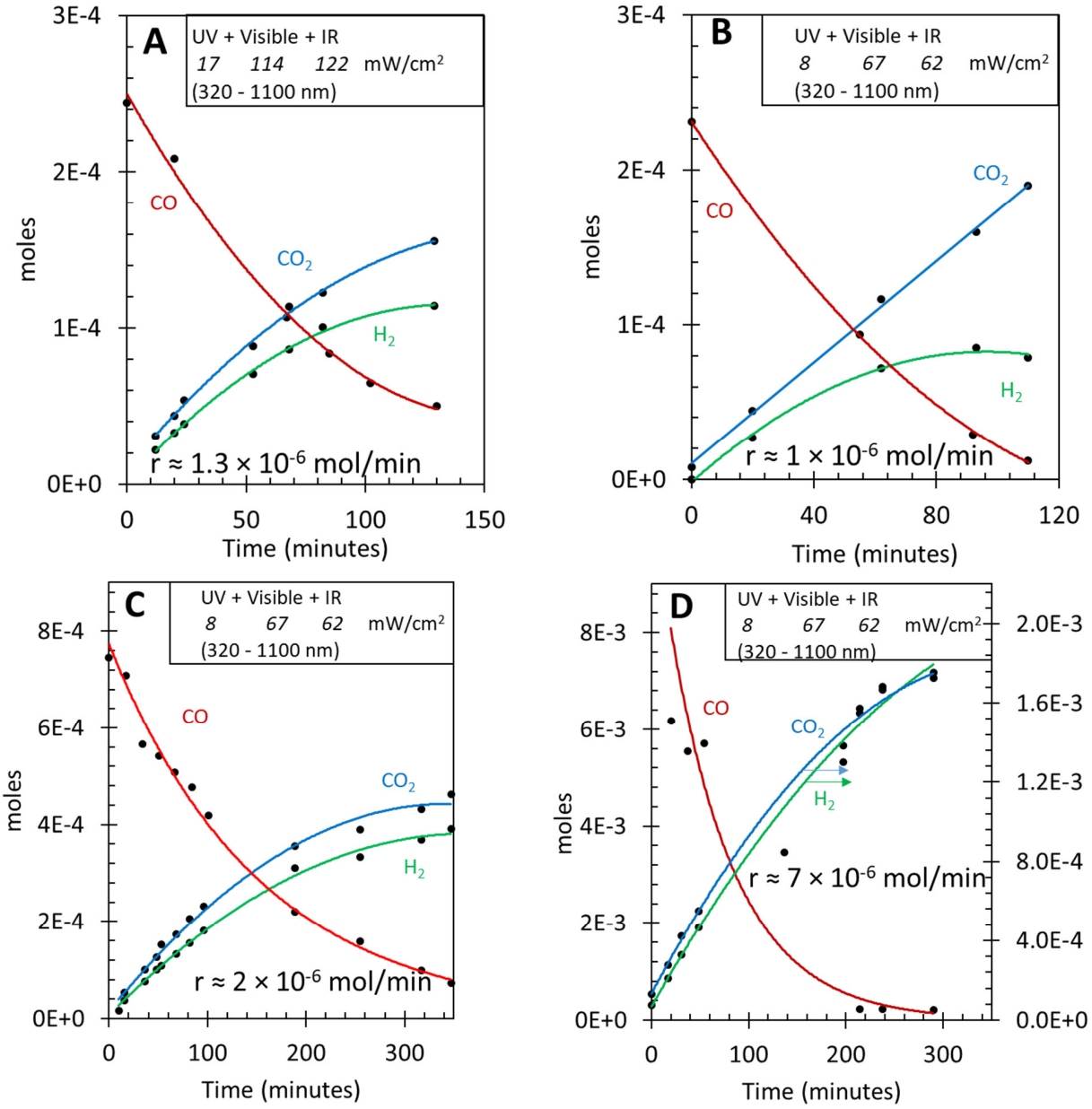

Figure 3. Effect of changing CO concentration on the H_2 to CO_2 ratio during the photo-thermal WGSR at 85 °C over 8 wt.% Au/TiO_2 P25. For all figures, the same light energy distribution was used. (**A**) CO_2 and H_2 production and CO consumption as a function of time with an initial CO concentration of ca. 2.5×10^{-4} mol. (**B**) The same reaction except for the fact that the light flux was decreased. (**C**) The same reaction as in B but with an increase in CO concentration to ca. 7.5×10^{-4} mol. (**D**) The same reaction as in B but with a further increase in CO concentration to ca. 7.5×10^{-3} mol.

To identify the effect of higher initial CO concentrations, a WGSR was carried out at higher CO concentration than that used in the experiments described above. In this experiment, the reactor was purged with CO instead of N_2 to decrease any possible outgassing from the wall of the reactor. Figure 3C presents the results for the WGSR under the same light energy and flux as those shown in Figure 3B. Figure 3C shows that the initial concentration of CO was three times that shown in Figure 3B, while that of water was the same. The initial rate of hydrogen doubled (2×10^{-6} mol/min) and became closer to that of CO_2 (2.4×10^{-6} mol/min). Figure 3D presents similar results but with an initial CO concentration of 5.8×10^{-3} mol, about 26 times that of Figure 3B (the CO to water ratio was near unity). Both CO_2 and H_2 production were virtually the same (with a ratio near unity), while the rate increased to 7×10^{-6} mol/min. To summarize the findings presented above, it appears that at a high concertation of CO (with negligible O_2 outgassing from the walls of the reactor) and when the ratio of CO/H_2O is near unity or above, the ratio of CO_2 to H_2 is near unity, too (see also Table 2). It is most likely that experimental artefacts are behind the sub-stoichiometric ratios observed by others.

Table 2. Effect of Changing CO concentration on the H_2/CO_2 ratio during the photo-thermal WGSR over 8 wt.% Au/TiO_2 P25.

[CO]	[H_2O]	Ratio [H_2O]/[CO]	Initial $r_{(H2)}$ mol/min	Initial $r_{(CO2)}$ mol/min	Ratio [H_2]/[CO_2]
0.00022	0.0011	5.0	1.2×10^{-6}	1.5×10^{-6}	0.8
0.00067	0.0011	1.6	2×10^{-6}	2.4×10^{-6}	0.9
0.0058	0.0055	≈1	7×10^{-6}	6×10^{-6}	1.1

Cumulative analytical and experimental errors in rates and concentrations are about 10%.

Based on others' results [14] and our own, one may describe the reaction as follows. 1. UV light excites the TiO_2 catalyst and generates electron hole pairs; then, photo-excited electrons transfer from the conduction band of TiO_2 to Au particles, which is in line with some of our more recent work on TiO_2 and ZnO [44–48], and a reduction of H_2O takes place on Au particles or at the Au/TiO_2 interface to produce H_2. 2. The photo-generated holes oxidize CO to form CO_2 on TiO_2 or at the Au/TiO_2 interface; interface; the oxygen atom, to make CO_2, originates from dissociated water in the form of surface hydroxyls. Although both thermal and photocatalytic WGSRs occurred since the experiment was performed at 85 °C under UV light irradiation, the former was much weaker.

2.4. Photo-Assisted Water–Gas Shift Reaction at 85 °C: Effect of O_2 Concentration

The effect of injecting O_2 during the reaction is presented in Figure 4. The objective here was to observe the effect of any potential contamination of O_2 on the reaction rates since both hydrogen and CO oxidation can take place under photon irradiation as well as at 85 °C in the presence of a Au/TiO_2 catalyst. The reaction was induced with a ratio CO to water equal to 1 and with the same photon energy and flux as those used in Figure 3B–D. Initially, only the thermal reaction was conducted at 85 °C (the first 30 min or so in the figure); then, light was turned on. The rates for H_2 and CO_2 production increased and are like those observed in Sections 2.2 and 2.3 (within experimental reproducibility). At about 200 min, 2 mL of O_2 was injected into the reactor. This resulted in a very fast increase in CO_2 production and a very fast consumption of CO. The consumption of CO was, however, higher than the production of CO_2. This indicates that only a fraction of surface species that consumed CO reacted to CO_2. This may point to the buildup of formate species and seems to indicate that their kinetics are too slow at the photon flux used. Also, the decay of the H_2 production rate was found to be mild, much less than the rise in CO_2. This is unlike Pd and Pt, as indicated in the Introduction section, where both are highly active for hydrogen oxidation. The results are in line with the preferential oxidation activity of Au particles observed thermally, shown here under the effect of photons. After a few minutes of reaction in the presence of O_2, the rates for both products started to rise again;

they were, however, weaker. The rate of hydrogen production decreased by half, and that of CO consumption was about four times slower. Table 3 presents the rates of the three compounds before, during, and after O_2 introduction. It is interesting to note that after O_2 injection and possibly its total consumption, the three rates became identical, indicating that the WGSR had become the sole reaction. This might be because the surface/gas reaction reached equilibrium at this point and because the fraction of available sites for reactions had become constant.

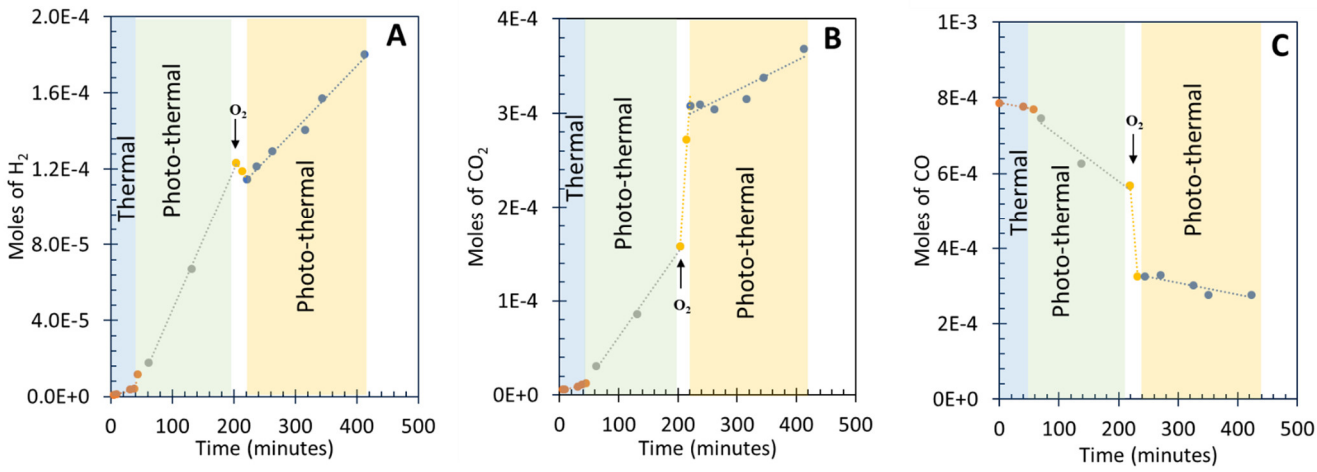

Figure 4. Effect of oxygen addition on the photo-thermal WGSR as a function of time over 8 wt.% Au/TiO_2 P25. (**A**) Hydrogen production. (**B**) CO_2 production. (**C**) CO consumption.

Table 3. Effect of O_2 addition (ca. 9×10^{-5} mol) on the reaction products and CO consumption during the photo-thermal WGSR over 8 wt.% Au/TiO_2 P25. The colours are used to highlight the three different regions during the reaction.

Before $r_{(H2)}$ mol/min	Before $r_{(CO2)}$ mol/min	Before $r_{(CO)}$ mol/min	During $r_{(H2)}$ mol/min	During $r_{(CO2)}$ mol/min	During $r_{(CO)}$ mol/min	After $r_{(H2)}$ mol/min	After $r_{(CO2)}$ mol/min	After $r_{(CO)}$ mol/min
0.75×10^{-6}	0.5×10^{-6}	-1.2×10^{-6}	-0.5×10^{-6}	11×10^{-6}	-19×10^{-6}	0.35×10^{-6}	0.35×10^{-6}	-0.35×10^{-6}

It is worth presenting, in a few equations, the possible reactions that took place.

There are two centers for reactions on the catalyst in the presence of light, namely, the semiconductor (TiO_2) and the metal (Au particles), including their interface. We will first address both separately for simplicity.

Upon light excitation, electrons are transferred from the valence band (VB) to the conduction band (CB) of TiO_2:

$$h\nu \rightarrow e(CB) + h(VB) \quad (5)$$

In the presence of gas-phase O_2, the latter reacts with e(CB) and becomes O_2^-, which may dissociate to O^- and an O atom.

$$O_2(g) + e^-(CB) \rightarrow O_2^- \rightarrow O\ atom + O^- \quad (6)$$

The oxygen atom reacts with CO, yielding CO_2, while the O^- may react with a proton of a surface OH group, yielding an OH radical (OH*). OH* are powerful oxidants. They then react with CO, yielding formats, and inject an electron into the VB.

$$CO + O\ atom \rightarrow CO_2(g) \quad (7)$$

$$O^- + OH(s) \rightarrow OH^* + O(s) \quad (8)$$

$$OH^* + CO(g) + h(VB) \rightarrow HOCO(a) \quad (9)$$

The sum of the above equations is Equation (10):

$$2\,CO(g) + O_2(g) + h\nu + OH(s) \rightarrow CO_2(g) + HOCO(a) + O(s) \quad (10)$$

Equations (7) and (9) may explain why the rate of disappearance of CO is twice that of the appearance of CO_2, since largely only one oxygen atom of molecular oxygen has reacted to give the CO_2 while the other gave a formate species (if the latter do not have a major role in the reaction at this temperature and light flux). While the initial decrease of hydrogen is due to oxidation to water. The origin of the second decrease after all oxygen had been consumed (compare the photothermal lines before and after oxygen injection) is unclear. A plausible explanation is that O_2 increases the concentration of formate species, and these have weak decomposition kinetics at the experimental conditions (Equation (9)), blocking some sites required for the regenerative mechanism to occur. This may indicate that, in reality, both mechanisms may occur and compete for the same sites.

The other route is that related to Au particles and their plasmonic effect (LSP). O_2 can dissociate on Au particles, yet this occurs on those with sizes below 2 nm or so [49–51]. The Au particles of the catalyst used here have a mean particle size of 5 nm (about 3000 atoms); while defects on these and the possible presence of some much smaller particles (not identified by TEM) may still have activity for the dissociative adsorption of O_2, their effect is neglected here. In particular, a recent time-dependent DFT computational study of Au particles with different sizes provided two important observations that might be relevant to this work [49]. First, it seems that under light excitation, particle size is not determinant, and second, O_2 dissociates largely because of the presence of an electric field effect and not via charge transfer. Based on these results, there are two distinct ways in which O_2 dissociation on Au/TiO_2 can occur either in the dark or under light excitation. 1. Dark dissociation seems to occur on small Au particles (<2 nm or so). 2. Light-induced dissociation can occur upon TiO_2 excitation (UV) followed by charge transfer to Au particles and/or upon LSPR that directly excites Au particles (largely via an electric field effect).

2.5. Photo-Assisted Water–Gas Shift Reaction at 85 °C: Effect of Light Energy

Figure 5 presents the data for the WGSR under light excitation with different energies at 85 °C. These light excitation modes were (UV + visible + IR), (UV + visible), and visible. Figure 5A shows hydrogen production under (UV + visible + IR) and (visible + IR). The light flux was kept constant as well as all other parameters. The rates are virtually the same. Therefore, it is clear that light with a wavelength below 400 nm (about 3 eV) is not needed. Since anatase TiO_2 absorbs light only below 400 nm, it is not directly implicated in the reaction. However, since P25 contains about 20% rutile TiO_2, it may still participate in the reaction. Figure 5B presents hydrogen production under similar light excitations but upon removing the late fraction of visible light and all IR light. The rates of hydrogen production under (UV + visible) (up to 620 nm) and visible excitation are very similar. Yet, in this case, the rate has decreased by about 40%. It is thus clear that light with a wavelength above 620 nm still affects the reaction rate. Figure 5C presents the same reaction only under visible light between 500 and 700 nm. These wavelengths excite Au particles only. The rate of hydrogen production is about a third of that in Figure 5A. However, when normalized to the number of photons used, the rate is higher than that obtained when using UV light to excite TiO_2 as well. Actually, when using light above 600 nm, the system still performs well. The straightforward conclusion is that a non-negligible fraction of the catalyst activity in this reaction is due to Au particles being directly excited by visible light, without requiring the use of UV light. Light with an energy level above 2 eV is not needed.

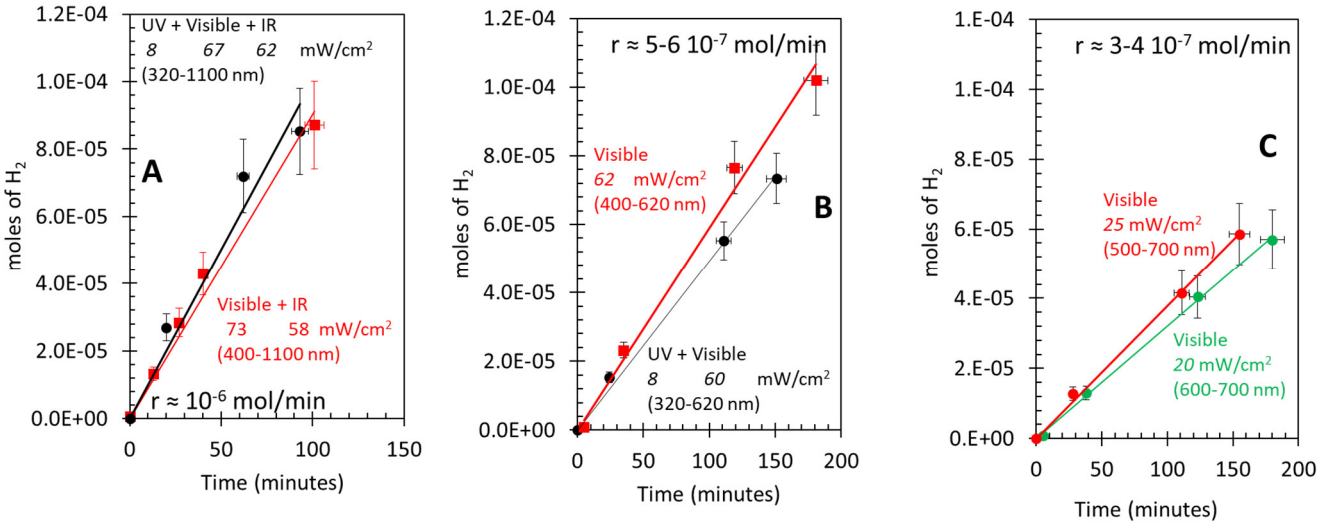

Figure 5. (**A**) Hydrogen production over 8 wt.% Au/TiO_2 P25 under "UV + visible + IR" and "visible + IR" with the indicated fluxes. (**B**) Hydrogen production over 8 wt.% Au/TiO_2 P25 under "UV + visible" (400–620 nm) and visible (400–620 nm) with the indicated fluxes. (**C**) Hydrogen production over 8 wt.% Au/TiO_2 P25 under visible light only in two regions (500–700 nm and 600–700 nm) with the indicated fluxes.

Based on the results found in this work, it appears that a Au/TiO_2 P25 catalyst composed of Au particles with an average size of 5 nm at a high enough surface density (3 at.% based on XPS, and about 10% per particle size based on TEM) and with a plasmon extending from 400 to 900 nm (centered at about 560 nm) presents activity for a WGSR under visible light without requiring the use of UV light to excite TiO_2. The main barrier for the reaction is that pertaining to electron transfer (initially from CO) leading to the formation of molecular hydrogen (from the protons of surface hydroxyls). Water dissociates readily on TiO_2 and does not require the presence of Au particles. CO may adsorb on both TiO_2 surfaces (where the adsorption energy is less than 0.5 eV, depending on the coverage) and on Au particles [52–54]). Upon visible light excitation, the LSPR of Au particles occurs. Energetically speaking, this is an electronic transition from 5d to 6s bands. Electrons at the 6s level have sufficient energy to reduce the protons of -OH group to atomic hydrogen while CO recombines with an adsorbed oxygen, with a net result of injecting electrons into the 5d energy level. This is presented in Scheme 1 and in Equations (11)–(15).

$$\text{Au (LSPR)} + \text{visible light} \rightarrow \text{5d-6s transfer} \quad (11)$$

$$H_2O(a) + 2\,e^-\ (6s) \rightarrow 2H + O^{2-}(s) \quad (12)$$

$$O^{2-}\ (a) + 2\,h^+\ (5d) \rightarrow O(a) \quad (13)$$

$$O(a) + CO(a) \rightarrow CO_2\ (g) \quad \Delta H^o_f = -283\ \text{kJ/mol} \quad (14)$$

Total

$$H_2O + CO \rightarrow CO_2 + H_2 \quad \Delta H^o_f = -41\ \text{kJ/mol} \quad (15)$$

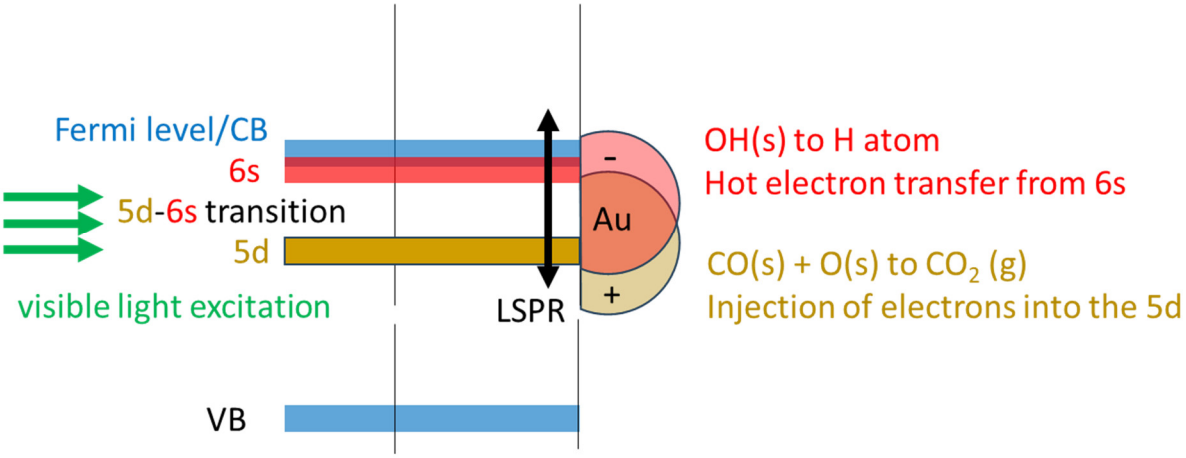

Scheme 1. A schematic representation of plasmon enhanced WGSR. The of the higher orbital levels of a gold nanoparticle (5s and 6d) together with the valence band, O2p, (VB) and conduction band, Ti3d, (CB) of TiO_2 are drawn. Upon visible light excitation (green arrows) excited electrons in Au nanoparticle (5d to 6s excitation, represented by a black vertical arrow)) may be transferred to the CB of TiO_2. This would result in the reduction of H^+ (of an -OH group at the interface Au/TiO_2) to a hydrogen atom (this process is repeated twice). At the valence band and adsorbed CO reacts with one O atom from the lattice to give CO_2 (the two electrons left regenerate the valence electrons); see Equations (11)–(13).

Schematic representation of Au LSPR effect on WGSR of a 8 wt.% Au/TiO_2 P25 catalyst. Au mean particle size is 5 nm. Visible light excitation of about 500–700 nm may enter into resonance with the 5d–6s band excitation of the Au atoms in the particles. These leave holes in the 5d and transfer electrons to the 6s/Fermi level. At the interface, Au/TiO_2 electrons may be transferred to protons of adsorbed water, while holes react with its oxygen anions. Note that CO oxidation is an exothermic reaction providing energy for the system. Therefore, the chemical input is provided by CO [55] (see Equations (11)–(15)).

The photo-catalytic reaction rate is a function of light flux and exposed area, while catalytic reactions are directly a function of the amount of matter. Therefore, a direct comparison may not be made easily without a devoted study focusing on quantifying the needed parameters for comparison, and this was not the objective of the study. A typical rate for low-temperature-WGSR Au catalysts is about 0.5 $mol/g_{(catal)}/h$ [56,57]. In the present study, the amount of matter was used in excess to avoid rate variations due to light matter interaction from one measurement to the other, so only the volumetric rate is considered.

3. Experimental Section

3.1. Preparation and Characterization of 8 wt.% Au/ P25 TiO_2

The $Au/P25$ TiO_2 photocatalyst was prepared as described previously [39]. Gold nanoparticles (8 wt.%) were deposited on Degussa P25 TiO_2 via the deposition–precipitation-with-urea method described by Zanella et al. [40], with some modifications. Briefly, $HAuCl_4{\cdot}3H_2O$ solution and urea were added to a glass Schott bottle and vigorously stirred. Degussa P25 TiO_2 was then added, and the resulting suspension was thermostated at 80 °C in a dark room for 8 h. After 8 h, yellow Au(III)-impregnated TiO_2 powder was collected via vacuum filtration, washed repeatedly with milli-Q water, and then air-dried at 70 °C overnight. The sample was then calcined at 300 °C for 2 h to thermally reduce the surface Au(III) species on TiO_2 to metallic gold.

The 8 wt.% Au/TiO_2 photocatalyst was characterized using transmission electron microscopy (TEM, JEOL Ltd., Tokyo, Japan), X-ray florescence (XRF, Bruker Corp., Billerica, MA, USA) spectroscopy, energy-dispersive X-ray (EDX) spectroscopy, X-ray diffraction (XRD, Rigaku Co., Yokyo, Japan), UV–visible spectroscopy (Shimadzu, Kyoto, Japan),

photoluminescence (Horiba, Kyoto, Japan), and X-ray photoelectron spectroscopy (XPS, Thermo Fisher Scientific, Waltham, MA, USA), and results were reported in a previous publication [39]. The average Au particle size derived from TEM images was ~5.1 nm. The UV–visible absorbance spectrum for the 8 wt.% Au/TiO_2 shows an intense absorption below 400 nm due to the P25 TiO_2 support and a broad absorption feature ~560–570 nm for the localized surface plasmon resonance (LSPR) of Au nanoparticles supported on TiO_2.

3.2. Photoreaction Setup

Photoreactions were carried out in a 140 mL flat bottom glass reactor. A total of 250 mg of Au/TiO_2 catalysts was dispersed on the bottom of the glass reactor. We opted to use excess catalyst so that the photocatalytic rate (which is also dependent on the number of photons hitting the catalyst) would have negligible rate variations from one run to the next. Water was added through a micro syringe over the catalyst powder. The reactor was then purged with N_2 to remove O_2 present in the system. After purging, a small amount of O_2, $\approx -6 \times 10^{-6}$ moles (wall outgazing), was present in the reactor. CO was then added to the reactor using a syringe to obtain the desired CO/H_2O ratio. All the photo-assisted WGSRs except one were performed at 85 °C in order to keep water in a vapor form. A Xenon lamp, Max 303 from Asahi spectra (Tokyo, Japan), was used as the light source for photoreactions. In some experiments, a CoolLED pE-4000 LED light source (CoolLED, Hampshire, UK) was used and applied to the sample using fiber optics. The reactants and products were analyzed using Gas Chromatography (GC). Hydrogen was analyzed with a Hayesep Q packed column at 45 °C and a Thermal Conductivity Detector (TCD) by using N_2 as a carrier gas. Oxygen, CO, and CO_2 gases were analyzed with a molecular sieve 5A column at 80 °C and TCD detector, using He as a carrier gas. Fluxes for the different forms of light used are given in Supplementary Materials (Figures S2–S8). All work was conducted at the corporate research center of SABIC at KAUST.

4. Conclusions

A WGSR over 8 wt.% Au/TiO_2 P25 (3 at.% Au/TiO_2 P25) was investigated thermally and in photo-thermal conditions. The latter was studied under light with different energies and fluxes. This was applied to investigate the effect of the localized surface plasmon (LSP) of the 5 nm mean size Au particles deposited on TiO_2 for the reaction and to de-couple it from that of the semiconductor support. In addition, the effects of CO concentration and O_2 addition during the reaction were investigated. The photocatalytic WGSR rate under light excitation with wavelengths extending from 320 to 1100 nm was found to be higher than that of the thermal reaction alone at the same temperature (85 °C). The expected ratio H_2/CO_2 of near unity was found only at high concentrations of CO. The rate of H_2 production was much less affected by the addition of O_2 than that of CO_2 production, indicating that Au/TiO_2 performs well for both WGSR and PROX under photo-irradiation. Probably the most notable result observed is that Au particles of 5 nm in size and when present in a high density over the semiconductor oxide support (about 10% particle density) showed equal activity under visible light (600–700 nm) compared to when UV light was also present. Therefore, we concluded that Au LSPR alone triggers this chemical reaction, without requiring the excitation of the semiconductor on which the Au particles are deposited.

Supplementary Materials: The following supporting information can be downloaded at https://www.mdpi.com/article/10.3390/catal13111444/s1. Figure S1: Transmission Electron Microscopy images of 8 wt.% Au/TiO2 P25 with different magnifications; Figure S2: Light flux as a function of wavelengths from 320 to 1100 nm (25% light intensity), Figure S3: Light flux as a function of wavelengths from 320 to 1100 nm (40% light intensity), Figure S4: Light flux as a function of wavelengths from 400 to 1100 nm (25% light intensity), Figure S5: Light flux as a function of wavelengths from 320 to 620 nm (25% light intensity), Figure S6: Light flux as a function of wavelengths from 400 to 660 nm (25% light intensity), Figure S7: Light flux as a function of wavelengths from 610 to 700 nm (LED with band

pass filter at 80% intensity), Figure S8: Light flux as a function of wavelengths from 570 to 610 nm (band pass filter 40% light intensity).

Author Contributions: Conceptualization, H.I.; methodology, H.I. and A.K.W.; formal analysis, H.I. and A.K.W.; investigation, A.K.W.; writing—original draft preparation, A.K.W.; writing—review and editing, H.I. and K.M.; supervision, H.I. All authors have read and agreed to the published version of the manuscript.

Funding: This research received no external funding.

Data Availability Statement: Data are available with H.I. and A.K.W. and can be provided upon direct request.

Conflicts of Interest: The authors declare no conflict of interest.

References

1. Ratnasamy, C.; Wagner, J.P. Water gas shift catalysis. *Catal. Rev.* **2009**, *51*, 325–440. [CrossRef]
2. Sakurai, H.; Ueda, A.; Kobayashi, T.; Haruta, M. Low-temperature water–gas shift reaction over gold deposited on TiO_2. *Chem. Commun.* **1997**, 271–272. [CrossRef]
3. Sandoval, A.; Gómez-Cortés, A.; Zanella, R.; Díaz, G.; Saniger, J.M. Gold nanoparticles: Support effects for the WGS reaction. *J. Mol. Catal. A Chem.* **2007**, *278*, 200–208. [CrossRef]
4. Chen, Y.; Wei, Z.; Chen, Y.; Lin, H.; Hong, Z.; Liu, H.; Dong, Y.; Yu, C.; Li, W. Metal-semiconductor catalyst: Photocatalytic and electrochemical behavior of Pt-TiO_2 for the water-gas shift reaction. *J. Mol. Catal.* **1983**, *21*, 275–289.
5. Tabakova, T. Recent advances in design of gold-based catalysts for H_2 clean-up reactions. *Front. Chem.* **2019**, *7*, 517. [CrossRef] [PubMed]
6. Fu, X.-P.; Guo, L.-W.; Wang, W.-W.; Ma, C.; Jia, C.-J.; Wu, K.; Si, R.; Sun, L.-D.; Yan, C.-H. Direct identification of active surface species for the water–gas shift reaction on a gold–ceria catalyst. *J. Am. Chem. Soc.* **2019**, *141*, 4613–4623. [CrossRef] [PubMed]
7. Shido, T.; Iwasawa, Y. Regulation of reaction intermediate by reactant in the water-gas shift reaction on CeO_2, in relation to reactant-promoted mechanism. *J. Catal.* **1992**, *136*, 493–503. [CrossRef]
8. Tabakova, T.; Boccuzzi, F.; Manzoli, M.; Sobczak, J.W.; Idakiev, V.; Andreeva, D. A comparative study of nanosized IB/ceria catalysts for low-temperature water-gas shift reaction. *Appl. Catal. A Gen.* **2006**, *298*, 127–143. [CrossRef]
9. Plata, J.J.; Romero-Sarria, F.; Suárez, J.A.; Márquez, A.M.; Laguna, Ó.H.; Odriozola, J.A.; Sanz, J.F. Improving the activity of gold nanoparticles for the water-gas shift reaction using TiO_2–Y_2O_3: An example of catalyst design. *Phys. Chem. Chem. Phys.* **2018**, *20*, 22076–22083. [CrossRef]
10. Wang, J.; Kispersky, V.F.; Delgass, W.N.; Ribeiro, F.H. Determination of the Au active site and surface active species via operando transmission FTIR and isotopic transient experiments on 2.3 wt.% Au/TiO_2 for the WGS reaction. *J. Catal.* **2012**, *289*, 171–178. [CrossRef]
11. Burch, R.; Goguet, A.; Meunier, F.C. A critical analysis of the experimental evidence for and against a formate mechanism for high activity water-gas shift catalysts. *Appl. Catal. A Gen.* **2011**, *409*, 3–12. [CrossRef]
12. Sun, K.; Kohyama, M.; Tanaka, S.; Takeda, S. Reaction mechanism of the low-temperature water–gas shift reaction on Au/TiO_2 catalysts. *J. Phys. Chem. C* **2017**, *121*, 12178–12187. [CrossRef]
13. Zhang, X.; Xue, J.; Yue, M.; Qian, M.; Xia, S.; Ni, Z. Reaction mechanism of water gas shift over Aun clusters: A density functional theory study. *J. Fuel Chem. Technol.* **2017**, *45*, 1473–1480. [CrossRef]
14. Sastre, F.; Oteri, M.; Corma, A.; Garcia, H. Photocatalytic water gas shift using visible or simulated solar light for the efficient, room-temperature hydrogen generation. *Energy Environ. Sci.* **2013**, *6*, 2211–2215. [CrossRef]
15. Sato, S.; White, J.M. Photoassisted water-gas shift reaction over platinized titanium dioxide catalysts. *J. Am. Chem. Soc.* **1980**, *102*, 7206–7210. [CrossRef]
16. Millard, L.; Bowker, M. Photocatalytic water-gas shift reaction at ambient temperature. *J. Photochem. Photobiol. A Chem.* **2002**, *148*, 91–95. [CrossRef]
17. Haruta, M.; Tsubota, S.; Kobayashi, T.; Kageyama, H.; Genet, M.J.; Delmon, B. Low-temperature oxidation of CO over gold supported on TiO_2, α-Fe_2O_3, and Co_3O_4. *J. Catal.* **1993**, *144*, 175–192. [CrossRef]
18. Schlexer, P.; Widmann, D.; Behm, R.J.; Pacchioni, G. CO oxidation on a Au/TiO_2 nanoparticle catalyst via the Au-assisted Mars–van Krevelen mechanism. *Acs Catal.* **2018**, *8*, 6513–6525. [CrossRef]
19. Green, I.X.; Tang, W.; Neurock, M.; Yates, J.T., Jr. Spectroscopic observation of dual catalytic sites during oxidation of CO on a Au/TiO_2 catalyst. *Science* **2011**, *333*, 736–739. [CrossRef]
20. Saavedra, J.; Whittaker, T.; Chen, Z.; Pursell, C.J.; Rioux, R.M.; Chandler, B.D. Controlling activity and selectivity using water in the Au-catalysed preferential oxidation of CO in H_2. *Nat. Chem.* **2016**, *8*, 584–589. [CrossRef]
21. Saavedra, J.; Doan, H.A.; Pursell, C.J.; Grabow, L.C.; Chandler, B.D. The critical role of water at the gold-titania interface in catalytic CO oxidation. *Science* **2014**, *345*, 1599–1602. [CrossRef] [PubMed]
22. Sangeetha, P.; Chang, L.-H.; Chen, Y.-W. Preferential oxidation of CO in H_2 stream on Au/TiO_2 catalysts: Effect of preparation method. *Ind. Eng. Chem. Res.* **2009**, *48*, 5666–5670. [CrossRef]

23. Leal, G.B.; Ciotti, L.; Watacabe, B.N.; da Silva, D.C.L.; Antoniassi, R.M.; Silva, J.C.M.; Linardi, M.; Giudici, R.; Vaz, J.M.; Spinacé, E.V. Preparation of Au/TiO_2 by a facile method at room temperature for the CO preferential oxidation reaction. *Catal. Commun.* **2018**, *116*, 38–42. [CrossRef]
24. Hartadi, Y.; Behm, R.J.; Widmann, D. Competition of CO and H_2 for active oxygen species during the preferential CO Oxidation (PROX) on Au/TiO_2 catalysts. *Catalysts* **2016**, *6*, 21. [CrossRef]
25. Bion, N.; Epron, F.; Moreno, M.; Mariño, F.; Duprez, D. Preferential oxidation of carbon monoxide in the presence of hydrogen (PROX) over noble metals and transition metal oxides: Advantages and drawbacks. *Top. Catal.* **2008**, *51*, 76–88. [CrossRef]
26. Yoshida, Y.; Izumi, Y. Recent advances in the preferential thermal-/photo-oxidation of carbon monoxide: Noble versus inexpensive metals and their reaction mechanisms. *Catal. Surv. Asia* **2016**, *20*, 141–166. [CrossRef]
27. Dai, W.; Zheng, X.; Yang, H.; Chen, X.; Wang, X.; Liu, P.; Fu, X. The promoted effect of UV irradiation on preferential oxidation of CO in an H_2-rich stream over Au/TiO_2. *J. Power Sources* **2009**, *188*, 507–514. [CrossRef]
28. Rodríguez-Aguado, E.; Infantes-Molina, A.; Talon, A.; Storaro, L.; León-Reina, L.; Rodríguez-Castellón, E.; Moretti, E. Au nanoparticles supported on nanorod-like TiO_2 as catalysts in the CO-PROX reaction under dark and light irradiation: Effect of acidic and alkaline synthesis conditions. *Int. J. Hydrogen Energy* **2019**, *44*, 923–936. [CrossRef]
29. Gomes Silva, C.; Juárez, R.; Marino, T.; Molinari, R.; García, H. Influence of excitation wavelength (UV or visible light) on the photocatalytic activity of titania containing gold nanoparticles for the generation of hydrogen or oxygen from water. *J. Am. Chem. Soc.* **2011**, *133*, 595–602. [CrossRef]
30. Khan, M.A.; Al-Oufi, M.; Toseef, A.; Nadeem, M.A.; Idriss, H. Comparing the reaction rates of plasmonic (Gold) and non-plasmonic (Palladium) metal particles in photocatalytic hydrogen production. *Catal. Lett.* **2018**, *148*, 1–10. [CrossRef]
31. Sun, N.; Song, J.; Tao, Q.; Kan, E.; Kuai, L. High-loading single-atom Pt/TiO_2 mesoporous catalysts for superior photocatalytic oxidation of benzyl alcohol. *Microporous Mesoporous Mater.* **2022**, *337*, 111949. [CrossRef]
32. Yang, J.; Guo, Y.; Jiang, R.; Qin, F.; Zhang, H.; Lu, W.; Wang, J.; Yu, J.C. High-efficiency "working-in-tandem" nitrogen photofixation achieved by assembling plasmonic gold nanocrystals on ultrathin titania nanosheets. *J. Am. Chem. Soc.* **2018**, *140*, 8497–8508. [CrossRef] [PubMed]
33. Shekhar, M.; Wang, J.; Lee, W.-S.; Williams, W.D.; Kim, S.M.; Stach, E.A.; Miller, J.T.; Delgass, W.N.; Ribeiro, F.H. Size and support effects for the water–gas shift catalysis over gold nanoparticles supported on model Al_2O_3 and TiO_2. *J. Am. Chem. Soc.* **2012**, *134*, 4700–4708. [CrossRef] [PubMed]
34. Williams, W.D.; Shekhar, M.; Lee, W.-S.; Kispersky, V.; Delgass, W.N.; Ribeiro, F.H.; Kim, S.M.; Stach, E.A.; Miller, J.T.; Allard, L.F. Metallic corner atoms in gold clusters supported on rutile are the dominant active site during water−gas shift catalysis. *J. Am. Chem. Soc.* **2010**, *132*, 14018–14020. [CrossRef]
35. Flytzani-Stephanopoulos, M. Gold atoms stabilized on various supports catalyze the water–gas shift reaction. *Acc. Chem. Res.* **2014**, *47*, 783–792. [CrossRef]
36. Yang, M.; Flytzani-Stephanopoulos, M. Design of single-atom metal catalysts on various supports for the low-temperature water-gas shift reaction. *Catal. Today* **2017**, *298*, 216–225. [CrossRef]
37. Beck, A.; Horvath, A.; Stefler, G.; Scurrell, M.S.; Guczi, L. Role of preparation techniques in the activity of Au/TiO_2 nanostructures stabilised on SiO_2: CO and preferential CO oxidation. *Top. Catal.* **2009**, *52*, 912–919. [CrossRef]
38. Ma, Z.; Tao, F.; Gu, X. Development of new gold catalysts for removing CO from H_2. *Heterog. Catal. Nanoscale Energy Appl.* **2014**, *7*, 217–238.
39. Jovic, V.; Chen, W.-T.; Sun-Waterhouse, D.; Blackford, M.G.; Idriss, H.; Waterhouse, G.I. Effect of gold loading and TiO_2 support composition on the activity of Au/TiO_2 photocatalysts for H_2 production from ethanol–water mixtures. *J. Catal.* **2013**, *305*, 307–317. [CrossRef]
40. Zanella, R.; Giorgio, S.; Shin, C.-H.; Henry, C.R.; Louis, C. Characterization and reactivity in CO oxidation of gold nanoparticles supported on TiO_2 prepared by deposition-precipitation with NaOH and urea. *J. Catal.* **2004**, *222*, 357–367. [CrossRef]
41. Al-Azri, Z.H.; Chen, W.-T.; Chan, A.; Jovic, V.; Ina, T.; Idriss, H.; Waterhouse, G.I.N. The roles of metal co-catalysts and reaction media in photocatalytic hydrogen production: Performance evaluation of M/TiO_2 photocatalysts (M = Pd, Pt, Au) in different alcohol–water mixtures. *J. Catal.* **2015**, *329*, 355–367. [CrossRef]
42. Jovic, V.; Smith, K.E.; Idriss, H.; Waterhouse, G.I. Heterojunction synergies in titania-supported gold photocatalysts: Implications for solar hydrogen production. *ChemSusChem* **2015**, *8*, 2551–2559. [CrossRef]
43. Keiski, R.L.; Desponds, O.; Chang, Y.-F.; Somorjai, G.A. Kinetics of the water-gas shift reaction over several alkane activation and water-gas shift catalysts. *Appl. Catal. A Gen.* **1993**, *101*, 317–338. [CrossRef]
44. Williams, O.B.J.; Katsiev, K.; Baek, B.; Harrison, G.; Thornton, G.; Idriss, H. Direct visualization of a gold nanoparticle electron trapping effect. *J. Am. Chem. Soc.* **2022**, *144*, 1034–1044. [CrossRef] [PubMed]
45. Yim, C.-M.; Lamoureux, P.S.; Mellor, A.; Pang, C.L.; Idriss, H.; Pacchioni, G.; Thornton, G. Size and Shape Dependence of the Electronic Structure of Gold Nanoclusters on TiO_2. *J. Phys. Chem. Lett.* **2021**, *12*, 8363–8369. [CrossRef] [PubMed]
46. Katsiev, K.; Harrison, G.; Al-Salik, Y.; Thornton, G.; Idriss, H. Gold cluster coverage effect on H_2 production over rutile TiO_2 (110). *ACS Catal.* **2019**, *9*, 8294–8305. [CrossRef]
47. Alsalik, Y.M.; Katsiev, K.; Idriss, H. Electron Transfer From a Semiconductor to a Metal and Its Implication on Photocatalysis for Hydrogen Production. *J. Phys. Chem. C* **2022**, *126*, 15184–15190. [CrossRef]

48. Ziani, A.; Al-Taweel, S.; Nadeem, M.A.; Idriss, H. Effect of Gold Loading on Time-Resolved ps Photoluminescence of ZnO. *J. Phys. Chem. C* **2022**, *126*, 16148–16157. [CrossRef]
49. Herring, C.J.; Montemore, M.M. Mechanistic Insights into Plasmonic Catalysis by Dynamic Calculations: O_2 and N_2 on Au and Ag Nanoparticles. *Chem. Mater.* **2023**, *35*, 1586–1593. [CrossRef]
50. Roldán, A.; Ricart, J.M.; Illas, F. Origin of the size dependence of Au nanoparticles toward molecular oxygen dissociation. *Theor. Chem. Acc.* **2011**, *128*, 675–681. [CrossRef]
51. Roldán, A.; González, S.; Ricart, J.M.; Illas, F. Critical size for O_2 dissociation by Au nanoparticles. *ChemPhysChem* **2009**, *10*, 348–351. [CrossRef] [PubMed]
52. Ramalho, J.P.P.; Illas, F.; Gomes, J.R. Adsorption of CO on the rutile TiO_2 (110) surface: A dispersion-corrected density functional theory study. *Phys. Chem. Chem. Phys.* **2017**, *19*, 2487–2494. [CrossRef] [PubMed]
53. Pursell, C.J.; Chandler, B.D.; Manzoli, M.; Boccuzzi, F. CO adsorption on supported gold nanoparticle catalysts: Application of the Temkin model. *J. Phys. Chem. C* **2012**, *116*, 11117–11125. [CrossRef]
54. Phala, N.S.; Klatt, G.; van Steen, E. A DFT study of hydrogen and carbon monoxide chemisorption onto small gold clusters. *Chem. Phys. Lett.* **2004**, *395*, 33–37. [CrossRef]
55. Idriss, H. Oxygen vacancies role in thermally driven and photon driven catalytic reactions. *Chem Catal.* **2022**, *2*, 1549–1560. [CrossRef]
56. Tao, F.F.; Ma, Z. Water–gas shift on gold catalysts: Catalyst systems and fundamental studies. *Phys. Chem. Chem. Phys.* **2013**, *15*, 15260–15270. [CrossRef]
57. Li, Y.-C.; Li, X.-S.; Zhu, B.; Zhu, A.-M. Boosting low-temperature water gas shift reaction over Au/TiO_2 nanocatalyst activated by oxygen plasma. *Chem. Eng. J.* **2022**, *430*, 133013. [CrossRef]